Substrate modification influence on properties of nanocomposite based on TiO_2 and gold nanoparticles

IOP Conf. Series: Journal of Physics: Conf. Series **1236** (2019) 012025 doi:10.1088/1742-6596/1236/1/012025

Substrate modification influence on properties of nanocomposite based on TiO_2 and gold nanoparticles

M V Mishin[1], A A Vorobyev[1], A S Kondrateva[1], E Y Koroleva[2], P A Karaseov[1], P G Bespalova[1], A L Shakhmin[1], A V Glukhovskoy[3], M C Wurz[3] and A V Filimonov[1]

[1] Peter the Great St. Petersburg Polytechnic University, Polytechnicheskaya 29, 195251, St. Petersburg, Russia
[2] Ioffe Institute, Polytechnicheskaya 26, 194021, St. Petersburg, Russia
[3] Institut für Mikroproduktionstechnik Produktionstechnisches Zentrum Leibniz Universität Hannover, An der Universität 2, 30823 Garbsen, Germany

E-mail: alex.spbpu@mail.ru

Abstract. In this work, we study photo-induced current transfer through nanocomposite structures consisting of the TiO_2 coating activated with plasmonic gold nanoparticles on top of pillar-like structured SiO_2. It is shown that the photo-response of the nanocomposite can be adjusted via tuning of the heterostructure topology. Processes at the interface between silicon and noble metal nanoparticle play an important role in charge carrier photo-generation. The high photo-activity in visible part of spectrum has been found in the composite, containing pillar-like silicon dioxide nanostructures [1]. The electron transport via the SiO_2 layer from the potential well at the TiO_2-SiO_2 interface to the n-Si conduction band was explained by electron tunneling mechanism. We present the empirical qualitative model which explains experimental results and helps to separate the contributions of different transport mechanisms.

1. Introduction

Various materials that can efficiently convert photon energy into electrical or chemical energy are of great interest to both researchers and practicing technologists since they have extensive possibilities for use in various kinds of devices. Two-dimensional (2D) systems based on transition metal oxides are systems with unique electronic properties, high specific surface area and demonstrate promising applications, ranging from electronics to energy storage [2]. A wide range of different electronic configurations and functionality successfully combined with their own stability (thermal, biological, etc.) [3].

However, the practical use of such materials is complicated by the fact that being wide-gap semiconductors they have an optical absorption range outside the visible part of spectrum. One way to circumvent this limitation is to create nanocomposite coatings based on a semiconductor matrix with embedded nanoparticles, in particular, from noble metals [4]. Such nanoparticles have the property of resonant excitation of surface plasmon oscillations, which ensures strong absorption in the visible region of spectrum [5]. The physics of photo stimulated processes occurring in such composite coatings is still not completely clear. Obtaining information about complex optoelectronic processes occurring in nanocomposite coatings based on semiconductor arrays with embedded metal particles is important for the developing of new nanomaterials with desired properties [4]. It has been shown [1]

that the introduction of metal nanoparticles with a plasmon resonance into matrix based on titanium oxide leads to photoactivity in the visible light range of this composite.

The purpose of this work was to study and establish the basic photoelectric properties of composite coatings based on titanium dioxide with gold nanoparticles.

2. Experimental

As an object of the study was choose a nanocomposite containing of a titanium dioxide (TiO_2) thin-film coating doped with gold nanoparticles (Au NPs) formed on silicon substrates with different surface modification.

2.1. Sample manufacturing

Production of samples took place in several stages. An array of gold nanoparticles was formed on pre-oxidized single-crystal silicon substrates (n-Si-4.5 of orientation [100]) to a depth of 35 nm, 80 nm and 130 nm. By the method of thermal spraying, 1.5 nm thickness gold layers were deposited on the substrates. Then the samples were heated for an hour at a temperature of 550 °C in an inert gas atmosphere. This led to the formation on the sample surface of a two-dimensional array of gold nanoparticles with a characteristic size of from 5 to 15 nm [1].

The pillar-like structures of the insulating SiO_2 underneath the gold particles [1] were etched by means of the deep reactive ion etching (DRIE) process prior to deposition of the TiO_2 layer. DRIE experiments were performed in an inductively coupled etching plasma (ICP180, Oxford Instruments) using Sulphur hexafluoride (SF_6) as an etching agent and octafluorocyclobutane (C_4F_8) for passivation. The experiments were focused on three parameters known to strongly influence the etch characteristics of interest: platen power during the etch step, the pressure (which was kept constant during the both steps to enhance stability), and duration of the passivation step. ICP power was fixed at the value of 700 W, which provides optimal plasma density. The duration of the etch step was fixed at 9 s. The etch steps were performed at low values of platen power (5W), at the pressure of 30 mTorr, followed by 5 seconds long passivation step. Etch time was 3minwhich provide etch depth of a few nanometers. The etch depth was measured using surface profilometry and an optical microscopy, the slope of the side walls were measured via the optical microscopy at the cleaved edge of a specimen.

At the final stage of samples fabrication, a TiO_2 layer was deposited on the formed structures using the CVD method (see figure 1(a)). The thickness of the TiO_2 layer was, on the order of 40 - 60 nm. The technique used for the formation of thin coatings of TiO_2 is given in [6]. Three types of samples, with different the height of silica columns: 30, 80, 130 nm were obtained.

2.2. Analysis methods

For samples analysis, an X-Ray photoelectron spectrometer Specs (Germany) was used. The spectra were obtained using the emission of the Mg_{Ka} line (1253.6 eV). The spectrometer was calibrated using the Au $4f_{7/2}$ gold line energy which was assumed to be 84.00 eV. The spectra of all samples were taken under identical conditions with the same hardware parameters.

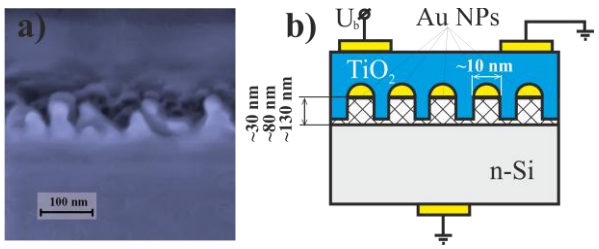

Figure 1. (a) typical SEM image of samples coated with TiO_2 (90° tilted view), (b) structure sketch of the sample used in this study.

The reflection spectra in the range of 200-900 nm were obtained using a UV-3600 Plus spectrometer. Surface image of samples were analyzed using the SEM SUPRA 55VP-25-78.

The current-voltage characteristics of the current flowing through the sample in the case of irradiating with varying light intensity and the current passing through the non-illuminated sample were recorded. LED was used as the light source. The emission spectrum of the LED was in the optical range, with an intensity maximum at a wavelength of 630 nm. The choice of the light source is due to the photoactivity of metal particles [7] in this region of the visible range and inactivity of semiconductor matrix whose photoactivity range is in the UV region [8]. The measurement was carried out at two values of illumination: $E_v$max = 50 lx and $E_v$min = 30 lx.

3. Results and discussion

3.1. XPS analysis

Samples were examined by XPS method. With the help of the developed technique on the stage of manufacturing, the position control of gold nanoparticles on the tops of the formed oxide pillars was monitored.

The qualitative and quantitative characteristics of the coating were investigated. The binding energy of the Ti $2p_{3/2}$ line corresponds to TiO_2 [9] (see figure 2(b)) and does not contain additional components indicating that the state of titanium atoms on the surface is different from TiO_2. This is also confirmed by the ratio of atomic concentrations of titanium and oxygen. For oxygen, only that part of the total atomic oxygen concentration is considered, which corresponds to the contribution of the decomposition component of the oxygen line spectrum corresponding to TiO_2 - 530.7 + \ - 0.2 eV (see figure 2(c)).

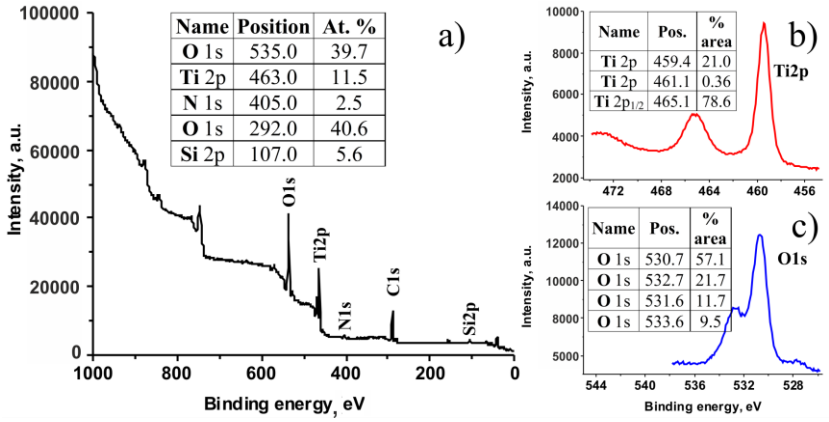

Figure 2. Typical XPS high resolution spectra of TiO_2 coating: (a) survey spectrum, (b) Ti 2p peak, and (b) O 1s peak. Gaussian lines used to fit experimental spectra are also drawn. Tables indicate positions and relative contributions of each individual component.

3.2. Electronic structure

Were obtained data that made possible to identify the features of the electronic structure in the surface layer of the nanocomposite (see figure 3). The estimation of the band gap of the surface layer of titanium oxide can be made from the shape of the spectrum of the Ti $2p_{1/2}$ line from the side of high binding energies. Photoelectrons emitted from this level of titanium atoms form a line on the spectrum if they released without losing energy. Electrons that have lost energy, during interaction, form an increasing background after the Ti $2p_{1/2}$ line from the side of high binding energies. The minimum possible energy loss for photoelectrons is the energy loss for the excitation of an interband transition between the top of the valence band and the bottom of the conduction band. On the spectrum, this corresponds to the beginning of the growth of the background of scattered electrons after the Ti $2p_{1/2}$ line from the side of high binding energies. The following data were obtained for the studied samples: nanocomposite - 3.9 eV; pure TiO_2 - 3.8 eV. The determination of the band gap from the spectrum in the region of the valence band is made difficult by accurately determining the top of the valence band. Approximately it can be expected at an energy of 2.6 eV relative to the Fermi level (see figure 3).

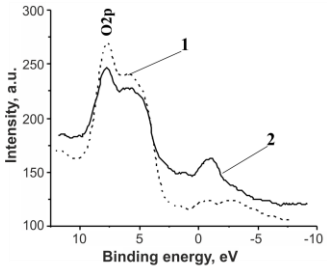

Figure 3. Comparison of XPS of valence band of TiO_2 grown on pure Si substrate (curve 1) and on the nanocomposite (curve 2).

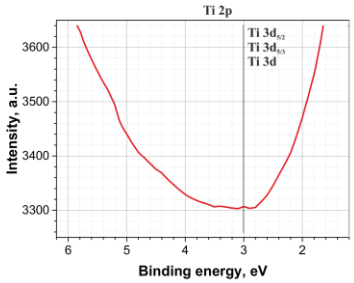

Figure 4. Spectra of energy losses.

Comparing the spectra of the valence band of the samples shows a significant difference in the intensity of the feature at -1.0 eV for the sample containing gold nanoparticles. As is known, the main channel for the loss of energy of electrons moving in a solid is the loss of plasmons excitation. The decay of plasmons is accompanied by the release of energy, which can be transferred to the electrons of the conduction band, forming an increase in the filling of levels at the bottom of the conduction band. This feature is located approximately 1.5 eV from the bottom of the conduction band, determined by the beginning of an increase in the signal intensity in the region of 0.5 eV.

Figure 4 presents the spectra of energy losses when the position of the photoelectron line is equal to 0. Accordingly, the first feature to the left of the line will correspond to the least energy loss of electrons - the transition between the valence and the forbidden bands. After the Ti $2p_{1/2}$ line transition energy is 3.6-3.8 eV.

3.3. Angular dependencies

The angular dependences of the Au / Si ratio and the angular position of the detector were obtained. presents the SEM micrograph of the SiO_2 pillar-like structure [1]. The results of XPS studies (see figure 5 left) with angular resolution supports the fact that the gold nanoparticles remained on the top of the pillar-like structure. The intensity of the signal on the graph was the ratio areas of the peaks Au4f / Si2p. The angle was read from the normal to the surface. The greater angle corresponded the smaller depth from the surface the electrons leave the material - surface sensitivity (see figure 5 right). Figure 5 presents the dependence which shows that the signal from electrons with energy corresponding to Au NPs increases with decreasing penetration depth. In this way, have been shown that Au NPs were located at the top of the pillar-like structure.

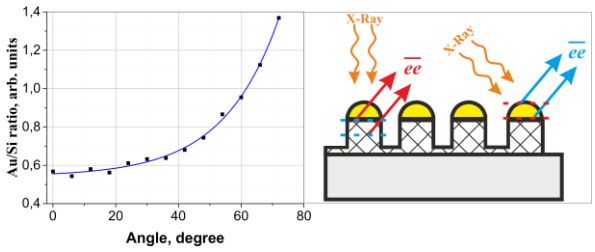

Figure 5. The angular dependence of the Au / Si ratio.

3.4. Optical analysis

Optical spectra of the radiation reflected from the samples in the range of 200-900 nm were obtained. The results are shown in figure 6. Spectra in the range of 300–350 nm are typical for TiO_2 and are given in numerous studies [10]. The spectra contain complex patterns, including features when radiation passes from a source through a layer of TiO_2 or nanocomposite and reflection of radiation

from the TiO_2 / Si interface. Thus, it is possible to observe a complex picture of absorbed and reflected radiation.

During the CVD process under the same conditions the amount of substance deposited on the substrate is the same, however, for samples with a more developed surface the thickness of the formed coating was less. This can explain the differences in the amplitude in the range 350-500 nm (see figure 6). A smaller coating thickness corresponds to a larger signal amplitude, which is caused by smaller losses in the transmission of radiation through TiO_2.

On the figure 6 reflection spectra of samples with pure TiO_2 and with the different etching depth of pillar-like structure are presented. For samples with Au NPs, absorption peaks were observed in the range of 450–650 nm (2–2.5 eV) which corresponding to peaks of plasmon absorption of Au NPs [11].

The plasmon excitation energy value obtained from the analysis of the energy structure was in the range of 1.0–2.0 eV from the bottom of the conduction band of TiO_2 (see figure 3). It corresponded to the energy range of 2.1 ± 2.3 eV. Plasmon optical absorption peaks ranged from 2.0–2.2 eV. Data from both methods of analysis well correlated with each other.

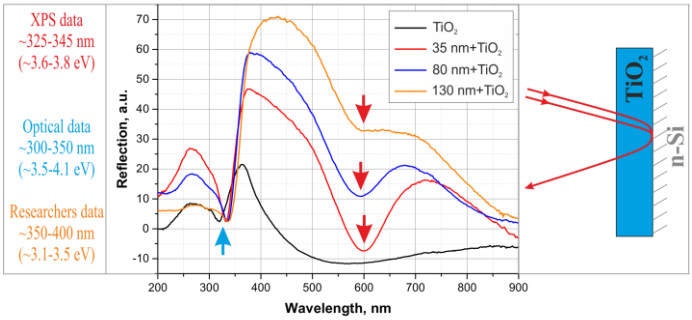

Figure 6. Optical reflection spectra of nanocomposite samples and pure TiO_2.

3.5. Electrical measurements

The current – voltage characteristics of different samples were obtained with and without irradiation. Figure 7 presents current – voltage characteristics of the samples with different etching depths of SiO_2 under a transverse bias. For the sample with 80 nm etching depth (see figure 7(a)) at the negative bias a significant effect of irradiation on the current – voltage characteristic was observed. The current increases almost 10 times under the influence of irradiation. In the absence of irradiation current practically absent up to the voltage of -5 V. With an increase of the irradiation intensity current increases nonlinearly. For samples with 80 nm etching depth (see figure 7(b)) the effect of irradiation was also observed, but not as strong as for 80 nm etching depth samples. The effect of irradiation for samples with 80 nm etching depth (see figure 7(a) inset) was absent.

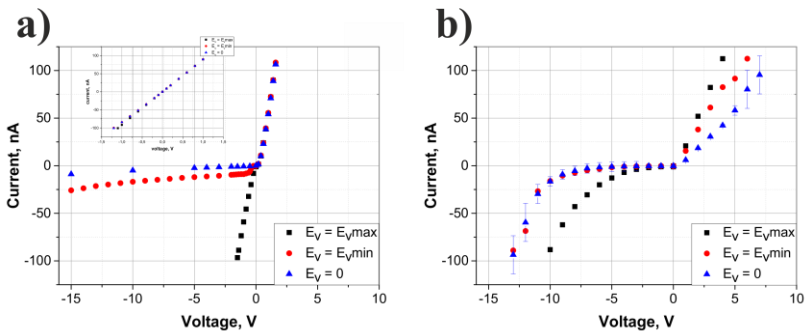

Figure 7. I–V characteristics of the samples with 80 nm (a) and 130 nm (b) etching depth obtained in the dark and under two illumination intensities at direct and reverse transverse bias U_b. The inset to figure 7(a) shows I–V characteristic of the 35 nm etching depth sample.

Figure 8 presents current – voltage characteristics of samples with different etching depths of SiO_2 under a longitudinal bias. For all types of samples was observed a significant effect of irradiation on the current-voltage characteristic. The strongest influence on irradiation was shown by samples with 35 nm etching depth (see figure 8(a)). As the etching depth of SiO_2 increased the effect of irradiation decreased. A significant nonlinearity of the current-voltage characteristics was observed, which is presumably associated with the connection of additional charge transport mechanisms, such as tunneling. Conventionally, dependencies can be divided into several sections. The following describes the proposed mechanism of charge transport under a longitudinal bias.

3.6. Model of charge transport mechanism

We proposed the model that qualitatively describes photo-induced transport processes in the heterojunction system [1]. The effects of electrical inhomogeneities and contribution of the Franz-Keldysh effect in the increase of TiO_2 charge carrier concentration was emphasized. This result can be used to describe behavior of charge-carrier generation of all samples. To describe charge transport mechanism, we assumed an electron tunneling transport mechanism through SiO_2.

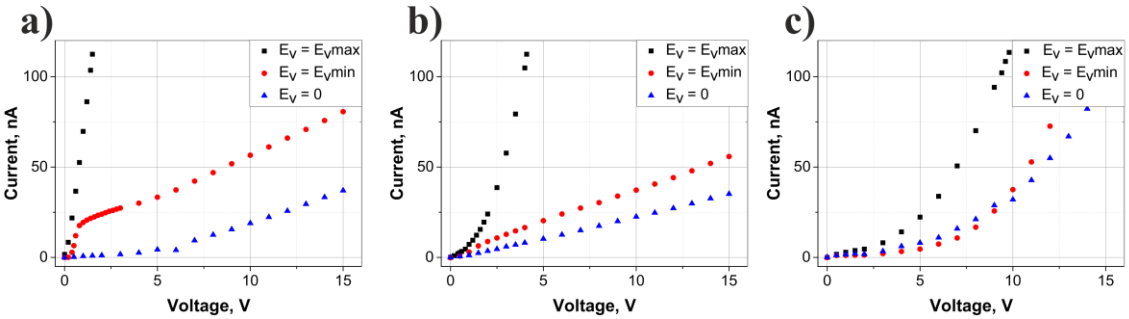

Figure 8. Current-voltage characteristics of the samples with 35 nm etching depth (a), 80 nm etching depth (b) and 130 nm etching depth (c) obtained in the dark and under two illumination intensities at longitudinal bias U_b.

The electron transport through the SiO_2 layer from the potential well at the TiO_2-SiO_2 interface to the n-Si conduction band can be determined via the approximation of the tunnel current equation (the case of an arbitrary shape barrier) [12]:

$$J = \frac{\alpha}{\delta_z^2}\{\bar{\varphi}\exp(-A\delta_z\sqrt{\bar{\varphi}}) - (\bar{\varphi} + eU_{ex})\exp[-A\delta_z\sqrt{\bar{\varphi} + eU_{ex}}]\}, \quad (1)$$

where α and A are numerical constants, $\bar{\varphi} = \frac{\varphi_1+\varphi_2}{2}$ is the mean height of the potential barrier, φ_1 is the work function of the potential well, φ_2 is the work function of n-Si, δ_z is the width of the potential barrier, U_{ex} is the potential drop at the barrier, β – correction factor.

At the low voltage $\bar{\varphi} \gg eU_{ex}\,(U_{ex} \approx 0)$expression (1) can be simplified to [19]:

$$J \cong \frac{\gamma\sqrt{\bar{\varphi}U_{ex}}}{\delta_z}\exp(-A\delta_z\sqrt{\bar{\varphi}}), \quad (2)$$

where $\gamma -$ is a constant.

Since $\bar{\varphi} \gg eU_{ex}$, we can assume that $\bar{\varphi}$ is independent of U_{ex}. Thus, if the applied voltage is small, the tunnel current is proportional to U_{ex}. This case is realized at the negative branch at low voltages (see figure 8).

If $\varphi_2 > eU_{ex}$ the tunneling current vs. voltage dependence takes the form:

$$J = \frac{\gamma\sqrt{\bar{\varphi}}}{\delta_z}\exp\left(-A\delta_z\sqrt{\bar{\varphi}}\right)(U_{ex} + \sigma U_{ex}^3), \quad (3)$$

where $\sigma = \frac{(Ae)^2}{96\bar{\varphi}\delta_z^2} - \frac{Ae^2}{32\delta_z\bar{\varphi}^{3/2}}$, $\bar{\varphi} = \frac{\varphi_1+\varphi_2-eU_{ex}}{2}$.

In this case current follows a power-law dependence on the voltage. it takes place in the segment of the I-V curve (see figure 8).

When the $\varphi_2 < eU_{ex}$ dependence (1) can be rewritten by inserting the expressions $\delta_z = L\varphi_1/(\varphi_1 - \varphi_2 + eU_{ex})$, $\bar{\varphi} = \varphi_1/2$ as:

$$J = \frac{e^3F^2}{8\pi^2\hbar\varphi_1\beta^2}\left\{\exp\left[-\frac{2\beta}{eF}\varphi_1^{\frac{3}{2}}\frac{\sqrt{2m}}{\hbar}\right] - \left(1 + \frac{2eU_{ex}}{\varphi_1}\right)\exp\left[-\frac{2\beta}{eF}\varphi_1^{\frac{3}{2}}\frac{\sqrt{2m}}{\hbar}\sqrt{1 + \frac{2eU_{ex}}{\varphi_1}}\right]\right\}, \quad (4)$$

where L – is the geometric thickness of the barrier, $F = U_{ex}/L$ is the electric field. In this case the current dependence on the voltage is exponential. In our experiments, this case was not achieved. At high illumination intensity, the measured current was limited by hardware (see figure 8). For a low illumination intensity, it can be assumed that the current was limited by the rate of photogeneration (see figure 8).

4. Conclusion

The TiO_2 - n-Si heterostructures were activated with gold nanoparticles in the visible part of the spectrum. The photoactivity of structures having different localization of activating nanoparticles was studied. The I-V characteristics were analyzed, in dependence of the sample illumination with visible light. The fundamental differences of the transport mechanisms were discovered for samples with different substrate modification. The models that satisfactorily describe photo induced transport processes in the heterojunction system were proposed. The contribution of Franz-Keldysh [13] effect in increase of the TiO_2 charge carrier concentration is pronounced. The electron transport through the SiO_2 layer from the potential well at the TiO_2-SiO_2 interface to the n-Si conduction band was determined via electron tunneling mechanism. The results of the work will help to improve photoactivity of the nanocoatings in visible spectrum and to design new one.

Acknowledgments

The authors are grateful M A Prosnikov for measuring optical spectra.

References

[1] Mishin M V, Vorobyev A A, Kondrateva A S, Koroleva E Y, Karaseov P A, Bespalova P G and Filimonov A V 2018 *Semiconductor Science and Technology* **33(7)** 075014
[2] Sun Z, Liao T, Dou Y, Hwang S M, Park M S, Jiang L and Dou S X 2014 *Nature communications* **5** 3813
[3] RUIZ PUIGDOLLERS A 2018 *Catalytic Properties of Zirconia: Role of Nanostructuring and Metal-Oxide Interface*
[4] Etrich C, Fahr S, Hedayati M, Faupel F, Elbahri M and Rockstuhl C 2014 *Materials* **7(2)** 727-741
[5] Cavas M, Gupta R K, Al-Ghamdi A A, Gafer Z H, El-Tantawy F and Yakuphanoglu F 2013 *Materials Letters* **105** 106-109
[6] Baryshnikova M, Filatov L, Mishin M, Uvarov A, Kondrateva A and Alexandrov S 2015 *physica status solidi (a)* **212(7)** 1533-1538
[7] Nakamura K, Oshikiri T, Ueno K, Wang Y, Kamata Y, Kotake Y and Misawa H 2016 *The journal of physical chemistry letters* **7(6)** 1004-1009
[8] Li J and Wu N 2015 *Catalysis Science & Technology* **5(3)** 1360-1384
[9] Wagner C D, Riggs W M, Davis L E, Moulder J. F and Muilenberg G E 1979 Handbook of X-ray Photoelectron Spectroscopy Perkin-Elmer Corp. *Eden Prairie MN* **38**
[10] Gupta G, Tanaka D, Ito Y, Shibata D, Shimojo M, Furuya K and Kajikawa K 2008 *Nanotechnology* **20(2)** 025703
[11] Han X, Liu Y and YinиY 2014 *Nano letters* **14(5)** 2466-2470
[12] Simmons J G 1963 *Journal of applied physics* **34(6)** 1793-1803
[13] Gol'dman A M, Zhdan E I and Sumaroka A G 1993 *J Exp Theor Phys* **57** 783–7